Electronic Supplementary Material (ESI) for Journal of Materials Chemistry A.

# High-Throughput Screening of Pd-based Quaternary Electrocatalyst for Oxygen Reduction Reaction in Alkaline Media

Jinyang Li, Helge S. Stein, Kirill Sliozberg, Jingbei Liu, Yanhui Liu, Genevieve Steric, Ellen Scanley, Alfred Ludwig, Jan Schroers, Wolfgang Schuhmann, and André D. Taylor

## Experimental

### Quaternary thin film preparation

The 300 nm thick quaternary thin film library was prepared using a magnetron co-sputtering system, on a 4 inch Si wafer (with a pre-sputtered 200 nm Cr adhesion layer). The thin-film library with a continuous compositional gradient was prepared at room temperature using four pure sputter targets (99.99% pure), with Pd, Au, Ag and Ti in a tetrahedral configuration in the co-sputtering system described previously.[1] Briefly, the Ti target was located perpendicular to the substrate in the co-sputtering system which is expected to generate a compositional spread with less variation. The base pressure before sputtering was below $10^{-7}$ mTorr. The thickness of the as-deposited thin film library was calculated by measuring individual sputtering rates before the deposition.

As sputtering was performed at room temperature without any subsequent heat treatment, a flat film morphology is assumed since the homologous temperature is well below 0.2 (assuming a melting point of about 2000 K of the material and a substrate temperature of 323 K due to thermal radiation from the sputter sources) using Thornton's and Anders Structure Zone Diagram (SZD).[2-4] According to Anders' SZD, there is likely to be an overall tensile strain. This assumption is based on the analysis that morphology is usually the same for one given crystal structure but changes at phase boundaries.[5]

### Compositional and Structural Characterization

The compositional mapping of the Pd-Au-Ag-Ti thin-film library was performed by an automated energy dispersive X-ray spectroscopy (Inca X-act, Oxford Instruments), sharing the same configuration of measurement area with the electrochemical measurement. Structural characterization of the entire library was conducted from $2\ \Theta = 30^{\circ}$ to $100^{\circ}$ at room temperature by using an automated scanning X-ray diffraction (XRD, Rigaku) with a Cu K$\alpha$ radiation source, in a rectangular array of 21 by 21 (441) measurement areas.

### Electrochemical characterization

The electrochemical high-throughput characterization was performed using an automated scanning droplet cell (SDC)[6, 7] on a 342 grid as shown in Fig. 1. The SDC mounted on a three-axes micropositioning system with high positioning accuracy of about 1 µm, contained a built-in double junction Ag/AgCl/3 M KCl/1 M KOH reference electrode (215 mV vs. NHE) and a Pt-wire counter electrode. The geometric measurement area (0.785 $mm^2$) was defined by the diameter of a tip of the SDC made of polytetrafluoroethylene (PTFE), which is pressed on the thin film materials library (ML). The ML was connected as working electrode to a potentiostat (Gamry Reference 600). The electrochemical cell was supplied by a syringe pump from a bottle of $O_2$ saturated 1 M KOH electrolyte.

The open-circuit potential (OCP) was measured first (500 s or until the stability criteria of 0.05 mV/s was fullfilled). Four conditioning CV between OCP and 0.635 V vs. RHE at 10 mV/s were followed by linear sweep voltammetry (LSV) from OCP to 0.635 V at 5 mV/s. Finally a 30 s long chronoamperometry (CA) at 0.635 V vs. RHE was performed to measure the mass transport limited ORR current. The deviation of the SDC surface area between the measurement areas was below 0.5%.[7] However, the use of KOH reduces the repeatability of the measurement area to around 5%, leading to an error bar of the measured current to about 5%. Data analysis was performed by means of the software package Origin. The open-circuit voltage was extracted by taking the average of the relatively stable region of the voltage plateau. The ORR overpotential was extracted from the intersection of the tangents between the baseline and the signal current. For internal comparison, the plateau currents were extracted by taking the average of the relatively stable region of voltage plateau.

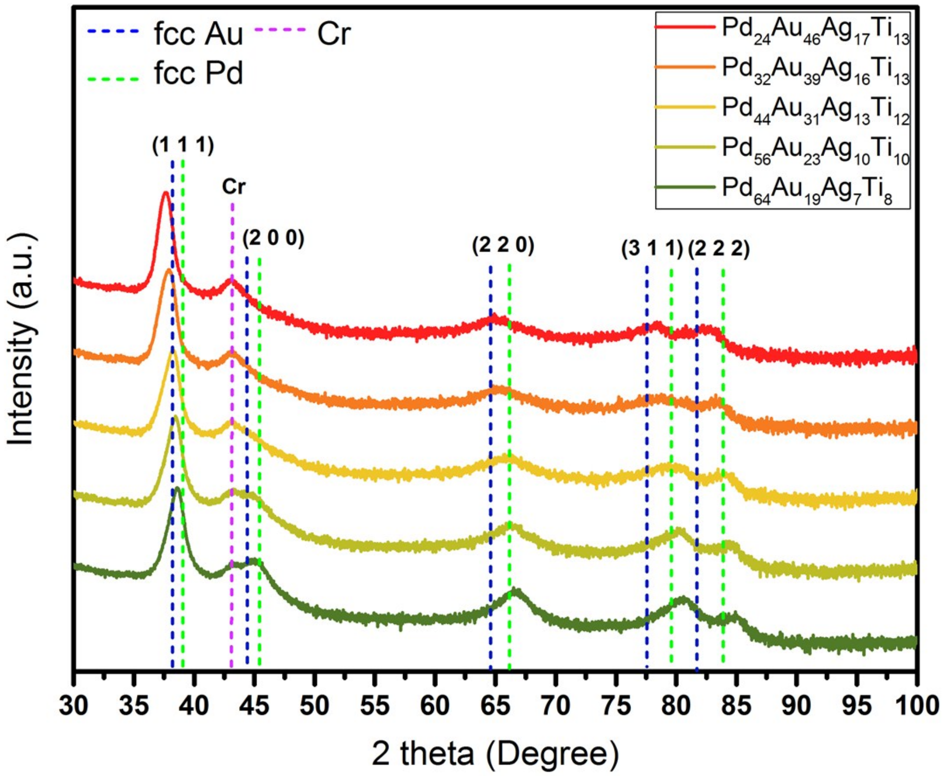

Fig. S1. Representative XRD patterns of the Pd-Au-Ag-Ti quaternary materials library with a decreasing Pd (increasing Au) content. All occurring peaks can be attributed to a fcc crystal structure. The Cr peak at around 43.2° is due to the adhesion layer deposited below the catalyst layer.

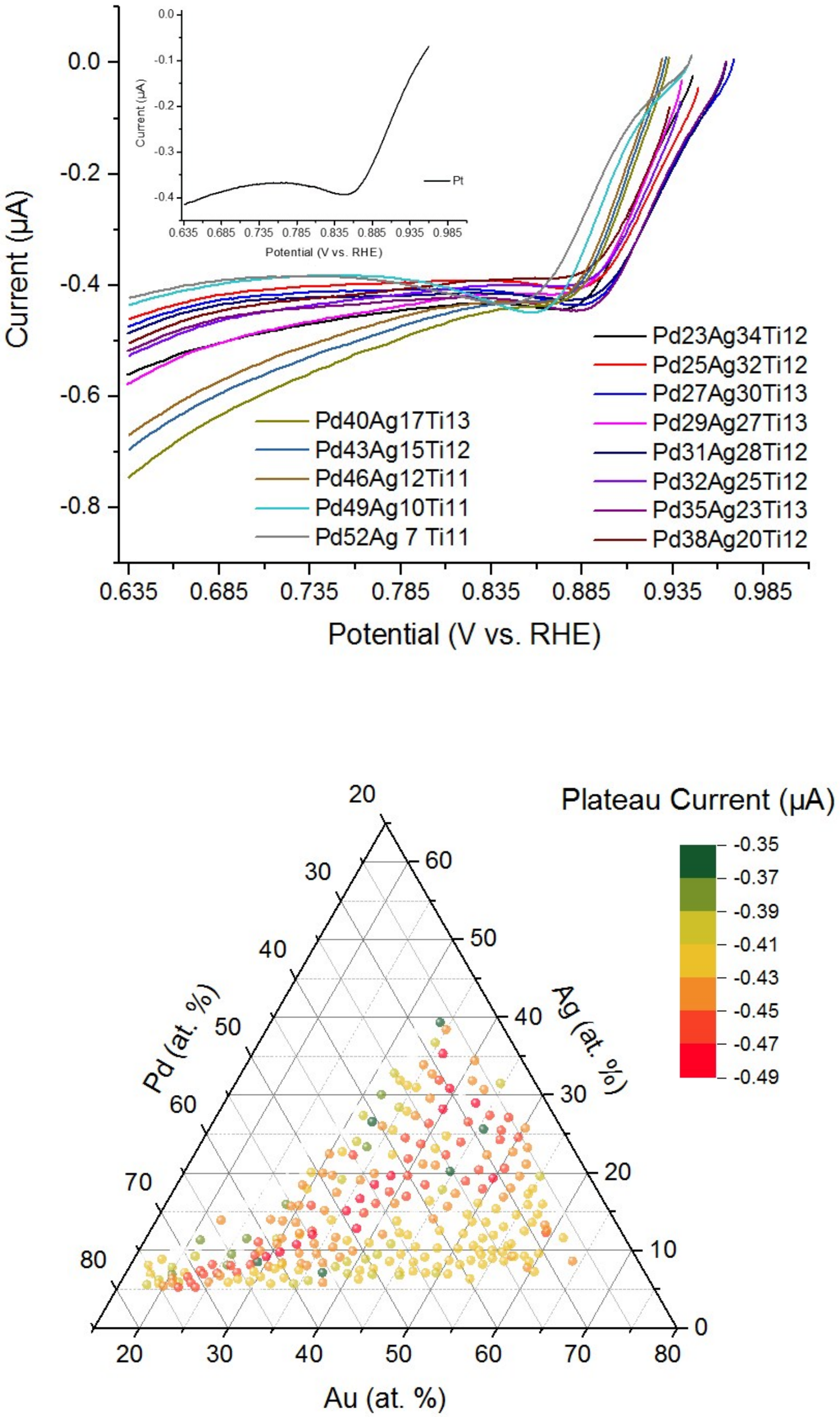

Fig. S2. (a) LSV curves with 30% Au (±1%) with the inlet of Pt film (b) The plateau current extracted from the LSV.

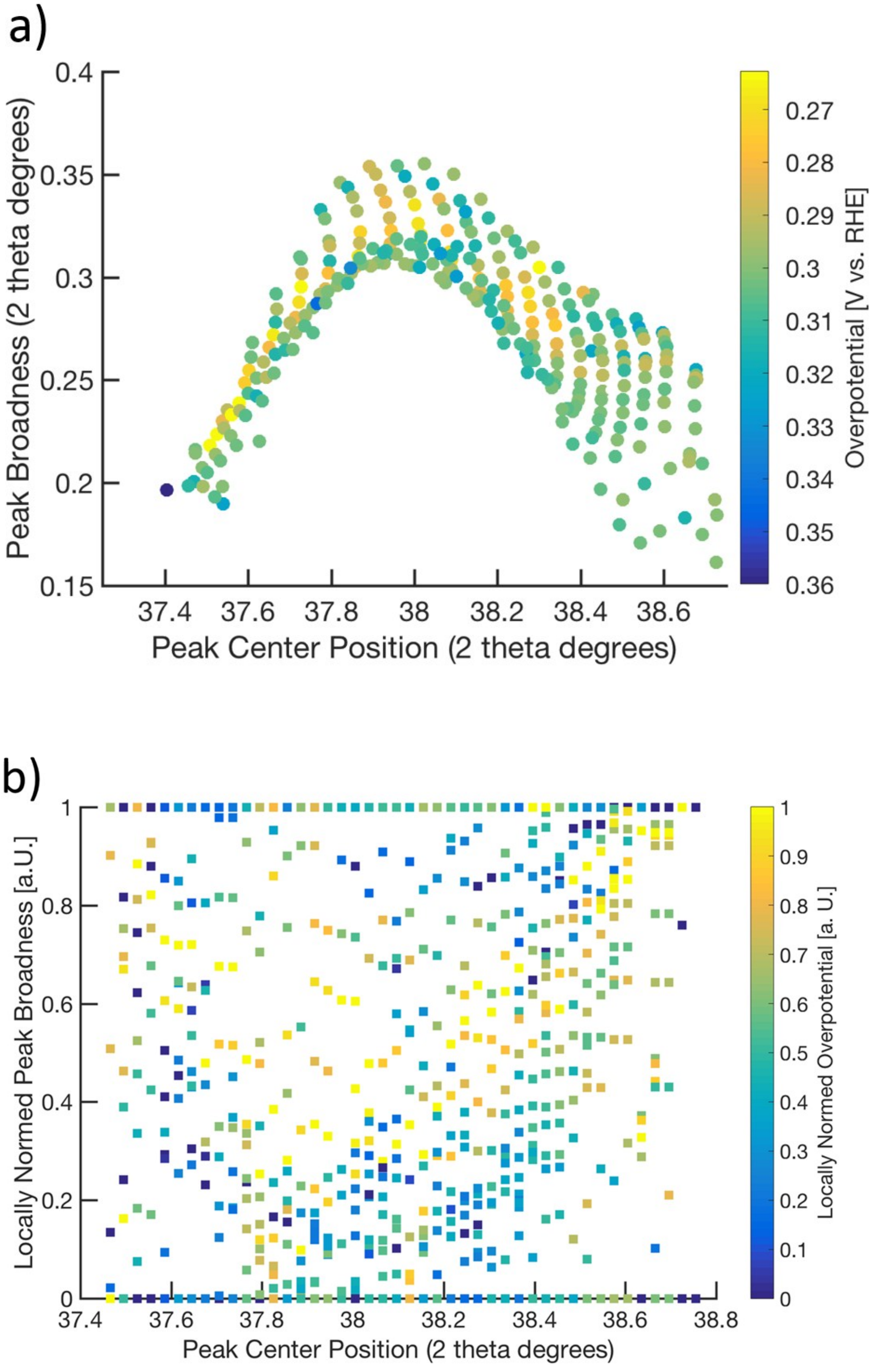
a)
Peak Broadness (2 theta degrees)
0.15
0.2
0.25
0.3
0.35
0.4
Peak Center Position (2 theta degrees)
37.4
37.6
37.8
38
38.2
38.4
38.6
Overpotential [V vs. RHE]
0.27
0.28
0.29
0.3
0.31
0.32
0.33
0.34
0.35
0.36
b)
Locally Normed Peak Broadness [a.U.]
0
0.2
0.4
0.6
0.8
1
Peak Center Position (2 theta degrees)
37.4
37.6
37.8
38
38.2
38.4
38.6
38.8
Locally Normed Overpotential [a. U.]
0
0.1
0.2
0.3
0.4
0.5
0.6
0.7
0.8
0.9
1

c)

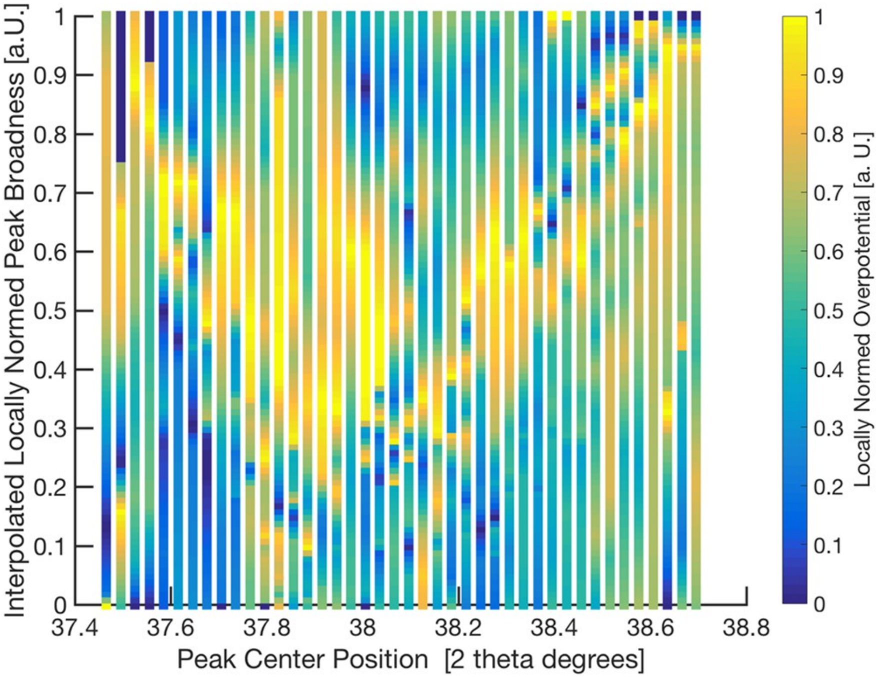

Fig. S3. Correlations between crystallography (x and y axis) and electrochemical data (overpotential - colorscale) yellow corresponds to a low and blue to a high overpotential. Refer to the manuscript text for detailed explanation.

To illustrate the correlation found between the crystallographic and electrochemical properties the plot of Figure 4 of the manuscript is shown in different representations in the Fig. S3. In Fig. S3 a) the same plot is shown just using another color scale. In Fig. S3 b) the same data is taken but in a modified way. For each center position $c \pm \varepsilon$ the peak width and overpotential are noralized so that the lowest value is 0 and the highest is 1. Then all data are plotted in Fig. S3 b) for all c with an increment of 0.03°.

For better visual representation the same data is taken but interpolated for each peak center position c to fill the white voids in Fig. S3 1c). This visualization (Fig. S3 1a / Figure 4) and its different representations (Fig. S3 b/c) suggest the same interpretation as in the manuscript that for each peak center position there is an optimal peak width / stress that usually lies in the middle of the local ($c \pm \varepsilon$) minimum and maximum of the peak width / stress. We also show different representations that correlates to the lattice constant from Vegards law vs. the measured one to validate the correlation in Fig. S3-S6.

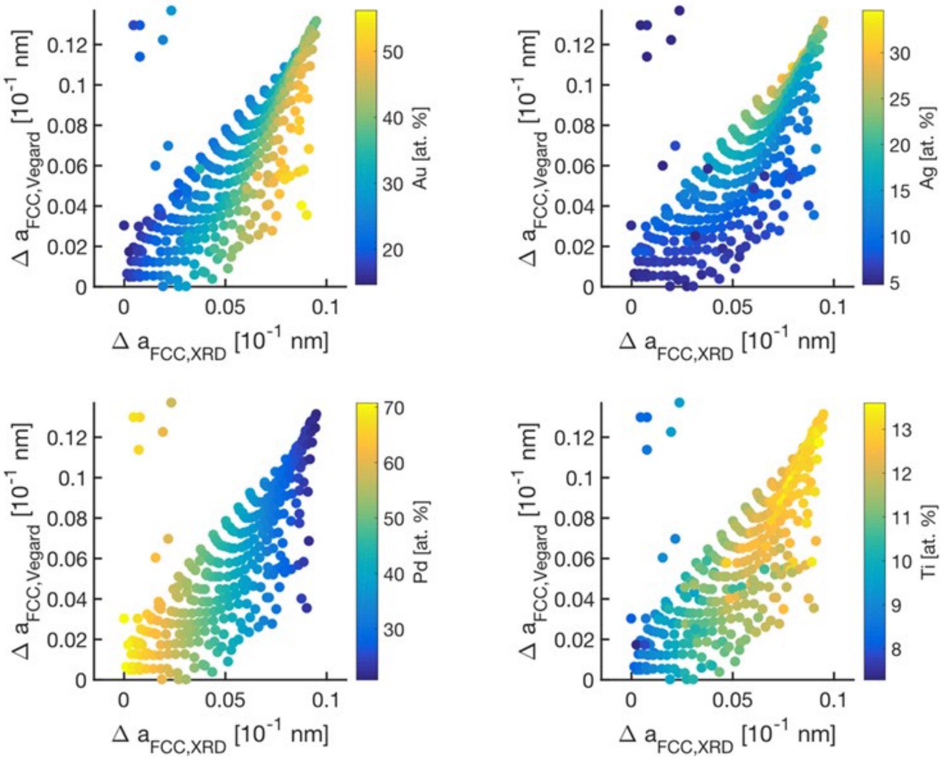

Fig. S4. Color-coded comparison of the Vegard’s law and XRD fcc (111) peak derived lattice constant with the respective concentration of each of the four elements shown. No evidence contradicting a fcc-solid solution is found.

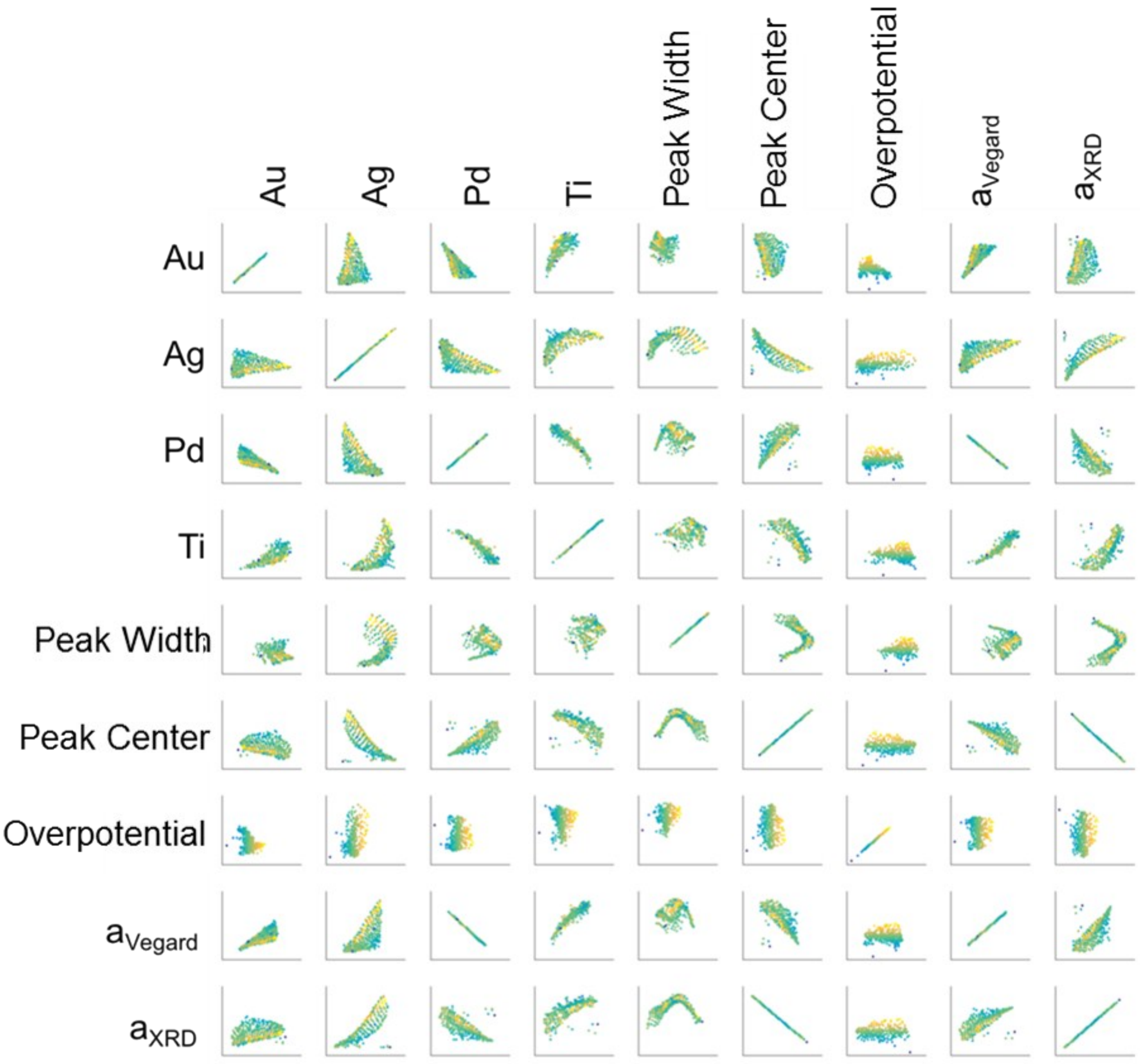

Fig. S5. Color coded overpotential pair-correlation plots showing that there is no simple elemental correlation of the overpotential with any of the other properties.

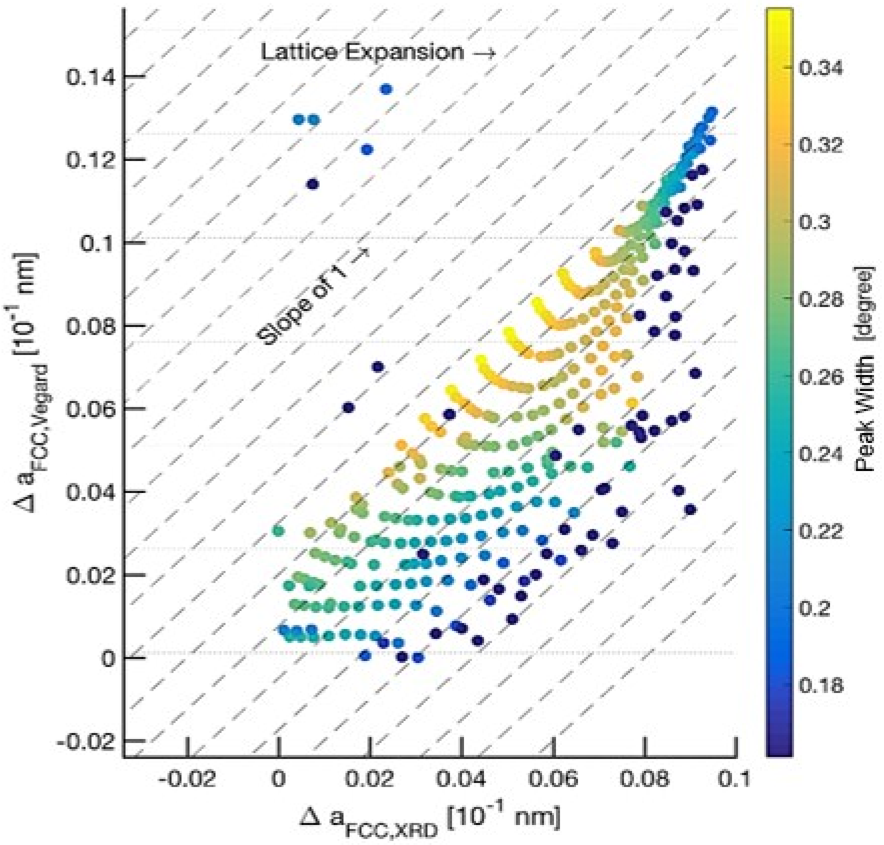

Fig. S6. Correlation of Vegards Law and XRD derived lattice constant with color coded peak width.

1. Y. Liu, J. Liu, S. Sohn, Y. Li, J. J. Cha and J. Schroers, *Nature Communications*, 2015, 6, 7043.
2. J. A. Thornton, *Journal of Vacuum Science and Technology*, 1974, 11, 666.
3. A. Anders, *Thin Solid Films*, 2010, 518, 4087-4090.
4. H. Stein, D. Naujoks, D. Grochla, C. Khare, R. Gutkowski, S. Grützke, W. Schuhmann and A. Ludwig, *physica status solidi (a)*, 2015, 212, 2798-2804.
5. R. Meyer, K. Sliozberg, C. Khare, W. Schuhmann and A. Ludwig, *ChemSusChem*, 2015, 8, 1279-1285.
6. K. Sliozberg, H. S. Stein, C. Khare, B. A. Parkinson, A. Ludwig and W. Schuhmann, *Acs Appl Mater Inter*, 2015, 7, 4883-4889.
7. K. Sliozberg, D. Schäfer, T. Erichsen, R. Meyer, C. Khare, A. Ludwig and W. Schuhmann, *ChemSusChem*, 2015, 8, 1270-1278.